Efficient boundary conditions for molecular statics models of solids

Xiantao Li*
Department of Mathematics, Pennsylvania State University, University Park, Pennsylvania 16802, USA
(Received 13 April 2009; revised manuscript received 26 June 2009; published 23 September 2009)

A method is presented for finding the boundary conditions for computer simulations based on molecular statics models. The boundary condition is expressed as a mapping from the atoms inside the boundary to the atoms outside and it models the effect of the surrounding atoms, which are too many to be modeled explicitly. The boundary condition is computed with a variational approach using lattice statics Green's functions as test functions. As examples, these boundary conditions are applied to systems with dislocations and cracks.

DOI: 10.1103/PhysRevB.80.104112 PACS number(s): 31.15.xv

I. INTRODUCTION

This paper is concerned with the boundary condition (BC) for numerical simulations based on molecular statics models. Such models typically involve a large number of atoms and the computation tends to be rather expensive. Therefore in practice, the computational domain is usually selected near the defects where the atomic deformation is large. Consequently artificial boundaries are created, where appropriate BCs have to be applied. Due to the nonlocal nature of static problems, the boundary may have a considerable effect on the simulation results.

A common approach is the fixed BC (or rigid BC), where one holds the atoms at the boundary at certain position. Since the atoms at the boundary are not allowed to move, artificial size effect will be introduced, and the results might depend strongly on the size of the system. For instance, many simulations of dislocations have shown the effect of the fixed boundary on the core structure unless the size of the system is sufficiently large.[1,2] To minimize the boundary effect, a more flexible boundary condition has been proposed by Sinclair *et al.*[1,3] The idea is to surround the computational domain with a buffer region that connects the computational domain to a continuum field. Then based on the excessive forces accumulated in the buffer region, one uses the Green's functions to adjust the position of the atoms in the entire system. This idea was later extended to three-dimensional (3D) systems by Rao *et at*.[2] Recent methods for calculating the Green's functions more accurately[4,5] makes this approach even more attractive.

The purpose of this paper is to develop an efficient BC for molecular statics. We start with the full molecular static model for the entire sample, from which atoms near the defects are selected to form a computational domain. We then eliminate the remaining degrees of freedom to reduce the dimension of the problem. This approach relies on the harmonic approximation for those surrounding atoms that will be removed. This idea has been explored by Karpov *et al.*[6] Using Fourier transform, they have derived the boundary condition in the form of a discrete convolution. This approach was later extended to single and multilayered graphite structures by Medyanick *et al.*[7]

The present paper proposes a BC that can be applied to boundaries of arbitrary geometry. It is expressed as a mapping from the atoms inside the computational domain to the outside atoms. The mapping is given by a sparse matrix. Such mapping corresponds to solving a linear problem in the outer region, which is still a problem too large to fit in a practical computation. But we will show that this difficulty can be overcome by an alternative representation, based on the lattice Green's functions. A variational formulation will be given, in which the Green's functions are used as test functions.

The form of the resulting BC is similar to the multiscale BC obtained by Karpov *et al.*[6] The derivation of the multiscale BC relies on Fourier transform and as a result the formulation only applies to planar boundaries. The main advantage of the multiscale BC is that it is expressed in terms of a kernel matrix, which is invariant along the boundary. However, this representation of the BC breaks down at corners. In order to retain the BC, additional atoms have to be reconstructed outside the corners by extrapolation.[7] The approach proposed here offers the flexibility of treating corners. Another practical issue is that the exact BC tends to be nonlocal: All the atoms near the boundary are coupled, which makes the implementation rather expensive. Fortunately it has been observed that the nonlocal dependence decays rather quickly as the distance between two the atoms at the boundary gets larger.[6] Therefore in Refs. 6 and 7 a cut off is introduced, neglecting the influence of the atoms outside the cut-off distance. In our approach, the local approximation is achieved with a variational formulation: assuming that an atom depends on L closest neighbors chosen from the interior, we find the optimal BC by minimizing certain error.

Meanwhile, this formulation, is different from the work of Sinclair *et al.*[1,3] and the following works,[2,4,5] which also use Green's functions. There they are used in the actual simulations to adjust the positions of the atoms outside *and* inside the boundary. The implementation requires the evaluation of the Green's functions and the displacement of *all* the atoms has to be adjusted every few steps while in our approach they are used prior to the simulation to obtain the BC; once the boundary condition is obtained, the implementation is quite easy. It does not require the access to the Green's function anymore. In addition, the local approximation makes the implementation much more efficient. To compare the computational cost, let M and N be the number of atoms at the boundary and the number of atoms in the computational domain, respectively. Then the flexible BC of Sinclair *et al.* requires $O(MN)$ evaluations of the Green's function. For the BC proposed here, the cost is $O(ML)$ operations of three-dimensional matrix-vector multiplications.

Although modern computers can treat a great number of atoms, the current BCs are still very useful. First, the implementation of the BC is straightforward. Second, since the derivation of the BC only depends on the bulk properties (the force constants) and the implementation only involves the coordinate of the nuclei, it can be used in simulations based on quantum-mechanical models, e.g., *ab initio* molecular dynamics. One such example can be found in the recent work,[8] where flexible BCs are implemented in the density-functional-theory calculation of dislocation structures. Third, we will show that the BC leads to a consistent linearization of the full interatomic potential. It simplifies the model so that the atomistic interaction is linearized in regions where the displacement is smooth while the full atomic description is still retained in critical areas near defects. Such technique will be useful for many other problems including dynamics problems.

Finally, similar issues also arise in dynamics problems, where the purpose of the BCs is to prevent boundary reflections. There has been a great deal of recent interest in developing nonreflecting BCs.[9–15] At zero frequency, such nonreflecting BC will reduce to the BC for static problems. In fact, many methods in this case, such as the damping method[16] and the perfectly matched layer method,[15] become the fixed or rigid BC, with only a few added layers, which will produce considerable error at low frequency. The method presented here can be extended to dynamics problems. This will be discussed in a forthcoming paper.

II. THE FORMULATION OF THE BOUNDARY CONDITION

We consider an atomistic system with N atoms, denoted by Ω, from which n atoms are selected to form the computational domain, denoted by Ω_I. The collection of the remaining atoms will be written as, Ω_J, $\Omega=\Omega_I\cup\Omega_J$. Such partition is demonstrated in Fig. 1. In most practical simulations, the dimension of Ω is much larger than that of Ω_I, $N\gg n$.

Let R_i be the reference position of atom i. This can be chosen based on the structure of a perfect crystal or based on an analytical solution of the corresponding anisotropic elastostatics problem. The current position is denoted by $\mathbf{r}_i$ with the displacement $\mathbf{u}_i=\mathbf{r}_i-R_i$. The energy of the entire system is modeled by a potential energy, V, which is written as

$$V(\mathbf{u}) = V(\mathbf{u}_I,\mathbf{u}_J). \tag{1}$$

Here $\mathbf{u}$ is the displacement of all the atoms, and $\mathbf{u}_I$ and $\mathbf{u}_J$ are respectively the displacement of the atoms inside and outside the computational domain. For molecular statics, one seeks the mechanical equilibrium by minimizing the total energy

$$\min_{\mathbf{u}} V(\mathbf{u}_I,\mathbf{u}_J). \tag{2}$$

Due to the large number of degrees of freedom associated with the entire system, such a problem is too large to fit in any practical computation. Therefore a reduction procedure is needed to reduce the size of the problem. For this purpose, we formulate this problem as a two-step minimization. In the first step, we consider

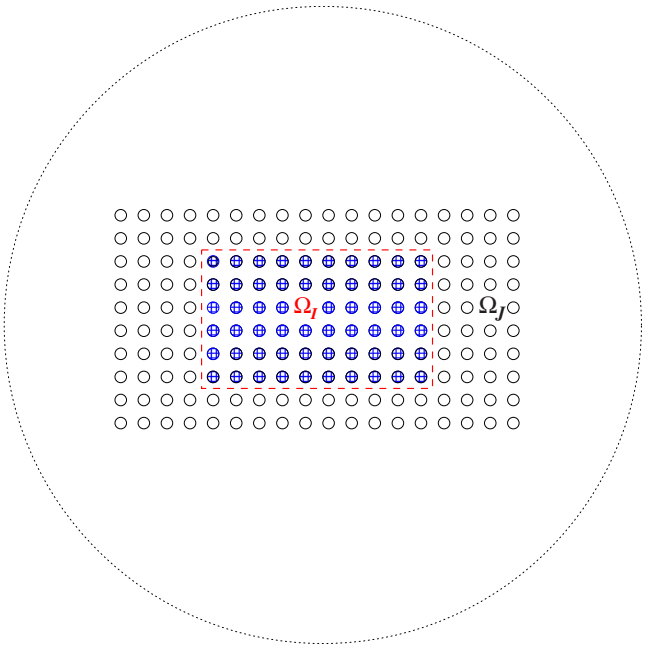

FIG. 1. (Color online) Schematic illustration of the partition of the system: the filled circles are the atoms included in the computational domain; the open circles are the outside atoms.

$$\min_{\mathbf{u}_J} V(\mathbf{u}_I,\mathbf{u}_J). \tag{3}$$

Alternatively, one may solve the nonlinear equation

$$\nabla_{\mathbf{u}_J} V(\mathbf{u}_I,\mathbf{u}_J) = 0. \tag{4}$$

The purpose of this step is to eliminate $\mathbf{u}_J$ from the system. In fact, let $\mathbf{u}_J^*$ be the corresponding solution, then in the second step, the energy becomes $V(\mathbf{u}_I,\mathbf{u}_J^*)$. The nonlinear equation is reduced to

$$\nabla_{\mathbf{u}_I} V(\mathbf{u}_I,\mathbf{u}_J^*) = 0, \tag{5}$$

which is a much smaller problem.

Although the first step dramatically reduces the atomic degrees of freedom, finding $\mathbf{u}_J^*$ from Eqs. (3) or (4) directly is still impractical. Therefore we make the following approximation: we linearize the interatomic force for those atoms outside the boundary. Such approximation is called the harmonic approximation.[17,18] The underlying assumption is that the displacement in the outer region is smooth. The interaction among the atoms inside the computational domain, on the other hand, is retained to model the defect structure. To explain this approximation more precisely, we let $D \in \mathbb{R}^{3N\times 3N}$ be the force matrix of the potential energy. An entry of D will be denoted by $D_{i,j}$ with the associated atoms i and j. The whole force matrix is partitioned according to the decomposition of the domain

$$D = \begin{bmatrix} D_{II} & D_{IJ} \\ D_{JI} & D_{JJ} \end{bmatrix}. \tag{6}$$

We then replace Eq. (4) by

$$D_{JI}\mathbf{u}_I + D_{JJ}\mathbf{u}_J = 0 \tag{7}$$

from which one finds

$$\mathbf{u}_J^* = B_{JI}\mathbf{u}_I, \quad B_{JI} = -D_{JJ}^{-1}D_{JI}. \tag{8}$$

The matrix B_{JI} defines a mapping from the inside atoms to the ones outside. It can be viewed as an interpolation operator that reconstructs the displacement of the outside atoms.

This procedure corresponds to approximating the total energy by

$$V \approx E_{\text{tot}} = V(\mathbf{u}_I, B_{JI}\mathbf{u}_I) + \frac{1}{2}(\mathbf{u}_J - B_{JI}\mathbf{u}_I)^T D_{JJ}(\mathbf{u}_J - B_{JI}\mathbf{u}_I). \tag{9}$$

Notice that the linear term has dropped out thanks to Eq. (4). Therefore this is a more flexible harmonic approximation which the full atomic interaction in the computational domain is still retained.

In the case when the potential energy is quadratic, it is equivalent to Schur complement. Namely, the energy after eliminating $\mathbf{u}_J$ is

$$V(\mathbf{u}_I, B_{JI}\mathbf{u}_I) = \frac{1}{2}\mathbf{u}_I^T(D_{II} - D_{IJ}D_{JJ}^{-1}D_{JI})\mathbf{u}_I.$$

Due to the dimension of D_{JJ}, it is still not practical to compute the mapping directly from Eq. (8). Therefore we will use an alternative expression. Let G be the inverse of D

$$G = D^{-1}, \tag{10}$$

which is partitioned accordingly

$$G = \begin{bmatrix} G_{II} & G_{IJ} \\ G_{JI} & G_{JJ} \end{bmatrix}. \tag{11}$$

Since G is the inverse of D, we have

$$D_{JI}G_{II} + D_{JJ}G_{JI} = 0.$$

Therefore, the mapping B_{JI} can be expressed in terms of the Green's function as follows:

$$B_{JI} = G_{JI}G_{II}^{-1}. \tag{12}$$

The Eq. (12) provides the basis for finding the boundary condition. This formulation is quite easy to implement, based on the following observation: (a) many atomic potential models have a cut-off radius, r_{cut}; an atom only interacts directly with other atoms within its cut-off radius. (b) Because of the short-range interaction, the matrix D_{JI} is sparse: only the entries corresponding to the atoms close to the boundary are nonzero. For the same reason, the inside atoms that are involved in B_{JI} are the ones that are next to the boundary. Meanwhile, in the next step, the forces in Eq. (5) only involve the outer atoms near the boundary. As a result, one just needs to compute a small number of entries in B_{JI}. (c) Because of the large size of the entire sample, the matrix G can be approximated by the Green's function for the full space, which will be discussed in the following section. (d) The Green's function can be efficiently computed with a Fourier integral, as described later.

Let $g_{i,k}$ be the (i,k) entry of G. This will be approximated by the full-space Green's function centered at atom k. The Eq. (12) can now be written as

$$\sum_{i\in\Omega_I} B_{ji}g_{i,k} = g_{j,k},$$

which has the following interpretation: if the inside atoms next to the boundary are displaced according to the Green's function centered at R_k, the displacement of the outside atoms should be given by the same Green's function. In addition, if all the atoms at the boundary are given a constant displacement, then this almost corresponds to a rigid translation of the entire sample. As a result, we have for any $j \in \Omega_J$

$$\sum_i B_{ji} = I.$$

This will be enforced as a constraint in our computation. From Eq. (8), we observe that $B_{ji}=0$, if the distance of atom i from the boundary is larger than the cut-off radius. In addition, with several numerical tests, we found that the entry also decays rapidly as the distance between atom i and atom j increases. Therefore we compute B_{JI} as follows: for each outside atom j whose distance from the boundary is less than r_{cut}, we choose several neighboring atoms from inside whose distance to atom j is less than a prescribed distance r_{min}. Based on their coordinate in the reference state, we compute the Green's functions and form the linear system Eq. (12). Another observation made was that along the straight edges of the boundary, the entries of B_{JI} remain the same. Therefore, we compute the matrix at the corners and then extend it along the edge until we arrive at another corner.

We now formulate the boundary condition as a variational problem

$$\min \left| \sum_{i,k} B_{ji}g_{i,k} - g_{j,k} \right|^2 \tag{13}$$

The minimization problem is solved by a least-square method. Once the mapping B_{JI} is obtained, the next step is to solve the Eq. (5). In practice, it is more convenient to solve the nonlinear equation by an energy minimization. Although there is a corresponding total energy V, the calculation requires the displacement of all the atoms. For empirical potential models, however, this can be simplified considerably. Notice that most interatomic potential can be written as

$$V = \sum_k V_k.$$

Namely, the energy can be defined for each atom. Based on this observation, we define the effective energy as

$$V_{\text{eff}} = \sum_{\text{dist}(R_k,\Omega_I)\le r_{\text{cut}}} V_k. \tag{14}$$

When $\mathbf{u}_J$ is held constant, one can easily show that

$$\nabla_{\mathbf{u}_I} V_{\text{eff}}(\mathbf{u}_I, \mathbf{u}_J) = \nabla_{\mathbf{u}_I} V(\mathbf{u}_I, \mathbf{u}_J). \tag{15}$$

Therefore, we will use V_{eff} as the approximate energy to help solving the nonlinear Eq. (5). This can be done as follows:

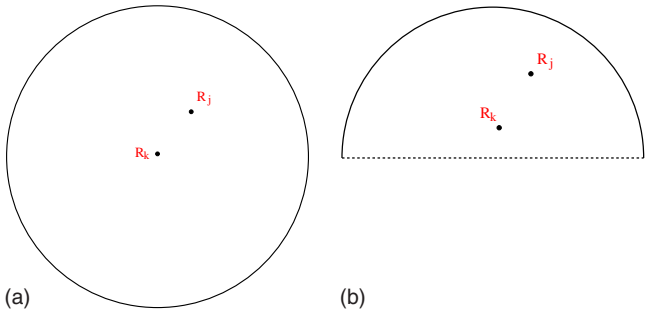

FIG. 2. (Color online) Green's function at R_j subject to a point force exerted at R_k. Top: the Green's function in the full space; bottom: the Green's function in the half space. The circle indicates an infinite system; the dash line shows a free surface.

we first hold $\mathbf{u}_J$ fixed and then minimize the effective energy. Upon convergence, we adjust $\mathbf{u}_J$ using the mapping B_{JI} and apply the minimization again. These steps will be iterated until certain convergence criteria are met. The minimization is done by the Broyden-Fletcher-Goldfarb-Shanno (BFGS) method.[19]

We may now compare our approach to the work of Sinclair *et al.*,[1,3] which also uses Green's functions. Both methods aim to eliminate the artificial forces accumulated at the boundary, thereby mimicking the behavior of a much larger system. The method of Sinclair *et al.* is based on the formula

$$\mathbf{u}_j = -\sum_k g_{j,k}\mathbf{f}_k,$$

which is derived for linearize models. Here $\mathbf{f}_k$ is the force on atom k at the boundary. Applying this formula, the region outside the computation domain automatically satisfies the force balance within the harmonic approximation. Since the atomic interaction inside the computational domain is nonlinear, this procedure has to be repeated until convergence is achieved. In contrast, our approach reconstructs the displacement of the outside atoms from the displacement of the atoms inside, instead of the forces. Once the mapping B_{JI} is obtained, the Green's functions are no longer needed in the simulation, which is more convenient in practice.

III. THE LATTICE STATICS GREEN'S FUNCTIONS

In this section, we describe the Green's function for molecular statics and how they can be efficiently computed. Such function serves as the fundamental solution of the lattice statics problems. It is particularly useful for studying the atomic deformation due to local defects, see the paper[20] for a more complete discussion. In order to treat full three-dimensional problems, we consider the Green's function in 3D with an applied point force, as demonstrated in Fig. 2. In addition, we also consider the Green's function for a half space, which is needed for boundary conditions near a free surface, e.g., a crack face, see Fig. 5.

A. The full-space Green's function

We first consider the Green's function subject to a point force applied at the point R_k. It is defined as the solution of the following equation:

$$\sum_j D_{i-j}g_{j|k} = \delta_{i,k}I. \tag{16}$$

The matrix I is the 3×3 identity matrix. Due to translational symmetry, we have $g_{j|k}=g_{j-k|0}$. Therefore, we will drop the second index and let $g_j=g_{j|0}$.

The Green's function may be computed in a bounded domain with periodic or fixed boundary conditions. However in 3D, such computation tends to be expensive and the results suffer from the boundary effect. A more efficient method is based on a representation of the Green's function as a Fourier integral. Let $g(\boldsymbol{\xi})$ be the Fourier transform of g_j

$$g(\boldsymbol{\xi}) = \sum_j e^{-iR_j\cdot\boldsymbol{\xi}}g_j. \tag{17}$$

Applying Fourier transform to Eq. (16), we get

$$g(\boldsymbol{\xi}) = D(\boldsymbol{\xi})^{-1}, \tag{18}$$

where $D(\boldsymbol{\xi})$, known as dynamical matrix,[17,18] is the Fourier transform of the force constant

$$D(\boldsymbol{\xi}) = \sum_j e^{-i\mathbf{R}_j\cdot\boldsymbol{\xi}}D_j. \tag{19}$$

As a result, we can express the Green's function as

$$g_j = \frac{1}{|\mathcal{B}|}\int_{\mathcal{B}} D(\boldsymbol{\xi})^{-1}e^{i\mathbf{R}_j\cdot\boldsymbol{\xi}}d\boldsymbol{\xi}, \tag{20}$$

where $\mathcal{B}$ is the first Brillouin zone and $|\mathcal{B}|$ is its volume.

Such Fourier integral is typically approximated by a quadrature formula with k points[21] as the quadrature points. One problem is that the acoustic branches of the phonon spectrum approaches to zero at the origin, which introduces a ξ^{-2} singularity, degrading the accuracy of the numerical integration. There are several methods to treat the singularity. This has been carefully studied in the recent work;[4] see Ref. 5 for numerical results on the convergence rates. To obtain better numerical accuracy, we will use the following techniques.

First, assuming that the system is a simple lattice, the dynamical matrix for small wavenumber has the asymptotic expansion of

$$D^{\mu\nu}(\boldsymbol{\xi}) = -\frac{1}{2}\sum_j D_j^{\mu\nu}(\boldsymbol{\xi}\cdot R_j)^2 + \cdots = \sum_{\alpha\beta}\Lambda C_{\alpha\mu\beta\nu}\xi_\alpha\xi_\beta + \cdots,$$

where

$$C_{\alpha\mu\beta\nu} = -\frac{1}{2\Lambda}\sum_{R_j} D_j^{\mu\nu}R_j^\alpha R_j^\beta$$

are the elastic constants[17,18] and Λ is the volume of the unit cell. Based on this asymptotic expansion, one finds that in the relative displacement

$$G_j - G_0 = \int_B D(\boldsymbol{\xi})^{-1}[\cos(\mathbf{r}_j\cdot\boldsymbol{\xi}) - 1]d\boldsymbol{\xi} \tag{21}$$

the singularity is removed. Since the dynamical matrix is positive definite, this equation also shows that for the diag-

onal entries of the Green's functions, the maximum should occur at the origin.

Second, using the asymptotic analysis,[22] one can show that for large R_j, the main contribution to the Fourier integral Eq. (20) comes from the origin. In particular, the Green's function should decay like $1/R$. Therefore, in our calculation, we compute the relative displacement, and then extract G_0 by fitting.

Finally, the Fourier representation Eq. (20) becomes a discrete sum in the numerical approximation and usually the resulting function is periodic, creating artificial images. Notice, however, the asymptotic expansion above agrees with that of the elastic Green's function. In fact, the leading term is the Christoffel matrix. Therefore in this case the lattice statics Green's function may be approximated by the elastostatic Green's function (multiplied by the volume of the unit cell, Λ), which can be formulated into an one-dimensional integral[23] and efficiently computed. A more accurate approximation based on higher order expansions can be found in Ref. 4.

As an example, we computed the Green's function for a body-centered-cubic (BCC) system. The results are plotted in Fig. 3 the lattice Green's function together with the elastic Green's function. We observe that the lattice Green's function starts to converge to the elastic Green's function when the distance is beyond 4–5 atomic spacings. Similar results were also found in Ref. 2.

B. The half-space Green's function

For a system with a free surface, e.g., an open crack, the boundary of the computational domain will intersect the surface, where the boundary conditions will be different from other parts of the boundary. In this case, we will derive the half-space Green's function as the test functions. Similar derivations for the continuum elastostatics model can be found in Refs. 24–26.

To compute such Green's functions, we consider a system in a half space containing all atoms for which, $R_j \cdot \mathbf{n} \geq 0$; $\mathbf{n}$ is the normal direction. For simplicity, we assume that the unit-cell vectors of the lattice are orthogonal and $\mathbf{n}$ coincides with the third direction. This can usually be achieved by choosing a large unit cell, which contains several atoms. Therefore the system is seen as a complex lattice. The Green's function is defined as the solution to the linear Eq. (16) with a point force applied to the $(0,0,k)$ cell. The traction at the boundary is zero.

Assuming that the lattice spacing in the three directions are a_1, a_2, and a_3. We first take a Fourier transform along the tangent planes, letting

$$U_j(\xi_1,\xi_2) = \sum_{R_k, R_k\cdot\mathbf{n}=ja_3} \mathbf{u}_k e^{-i(R_{k,1}\xi_1 + R_{k,2}\xi_2)}. \tag{22}$$

Similarly we let K_j and $G_{j|k}$ be the Fourier transform of the force constant and the full-space Green's function with the same center. For simplicity, we assume $K_j = 0$ for $|j| > 1$. This is usually the case since most atomic potentials have a cut-off radius about 2–4 atomic spacings and it can always be accomplished by choosing a large enough unit cell. The force

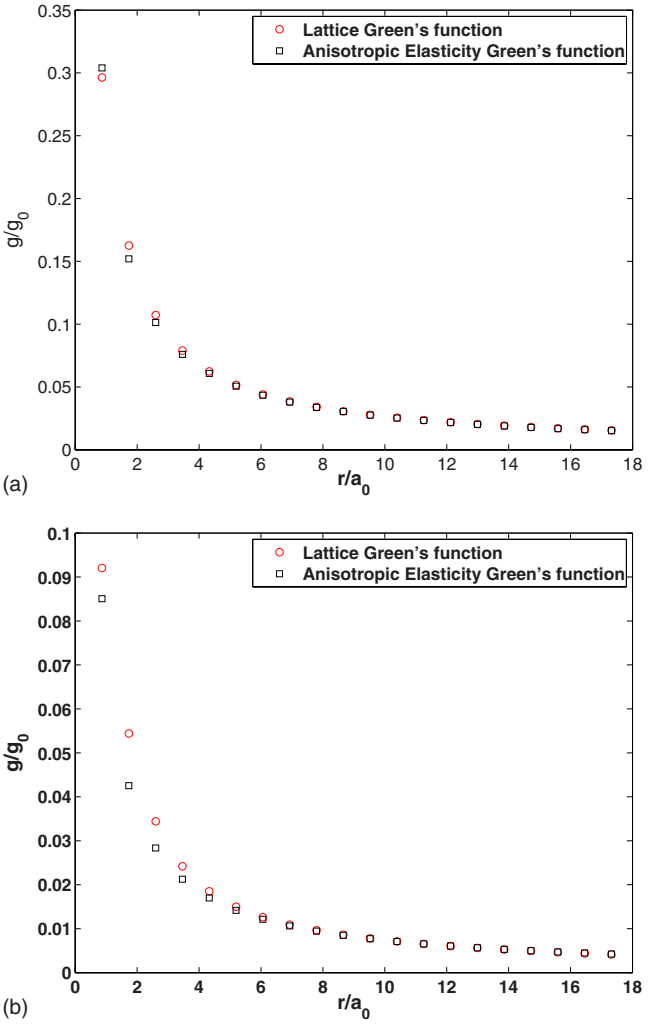

FIG. 3. (Color online) Full-space Green's functions along the ⟨111⟩ direction. Left: the diagonal (1,1) entries; right: the off-diagonal (1,2) entries. For comparison, the Green's functions for elastostatics are also plotted.

constant will be adjusted accordingly. They satisfy the symmetry property[17,18]

$$D_j = D_{-j}^T$$

from which, one finds that

$$K_j = K_{-j}^*, \tag{23}$$

where $*$ indicates complex conjugate.

After the Fourier transform, we obtain the following difference equation:

$$K_{-1}U_{j-1} + K_0 U_j + K_1 U_{j+1} = I\delta_{jk}, \quad j > 0. \tag{24}$$

For the homogeneous equation, one can seek a solution in form of

$$U_j = \lambda^j \boldsymbol{\varepsilon},$$

which leads to an eigenvalue problem

$$\det(K_{-1} + K_0\lambda + K_1\lambda^2) = 0 \tag{25}$$

and $\boldsymbol{\varepsilon}$ is the corresponding eigenvector.

To change the eigenvalue problem to a traditional form, we define the matrices

$$P = \begin{bmatrix} -K_{-1} & 0 \\ -\frac{1}{2}K_0 & I \end{bmatrix}, \quad Q = \begin{bmatrix} \frac{1}{2}K_0 & I \\ K_1 & 0 \end{bmatrix}. \tag{26}$$

Then the eigenvalue problem is turned into a generalized matrix eigenvalue problem

$$P\boldsymbol{\zeta} = \lambda Q\boldsymbol{\zeta} \tag{27}$$

in which $\boldsymbol{\zeta}=(\boldsymbol{\varepsilon}, \boldsymbol{\eta})^T$ and $\boldsymbol{\eta}=(\frac{1}{2}K_0+\lambda K_1)\boldsymbol{\varepsilon}$.

Due to the symmetry property Eq. (23), the roots will appear in pairs: if λ is a solution, so is $1/\bar{\lambda}$. In addition, let $\lambda=e^{-i\xi_3 a_3}$, then one finds that

$$K_{-1}\lambda^{-1} + K_0 + K_1\lambda = D(\xi_1, \xi_2, \xi_3).$$

Since the dynamical matrix is positive definite for any nonzero real wavenumber, ξ_3 must be complex unless $\xi_1=\xi_2=0$. Therefore in this case, the roots $|\lambda| \neq 1$. For each pair of roots, we choose λ so that $|\lambda|<1$. This guarantees that the solution approaches to zero as j goes to infinity. Thus the general solution can be written as

$$U_j = G_{j|k} + \sum \lambda_s^j \boldsymbol{\varepsilon}_s \otimes c_s = G_{j|k} + E\Lambda^j C.$$

Here Λ is a diagonal matrix containing the selected eigenvalues. The constant matrix C, the sth column of which is given by c_s, will be determined below.

To determine C, we first assume $k>0$. So at $j=0$, we have

$$K_0 U_0 + K_1 U_1 = 0.$$

Combining the above two equations, we get

$$\sum_s K_{-1} E\Lambda^{-1} = -K_{-1} G_{-1|k}.$$

Hence,

$$C = -\Lambda E^{-1} G_{-1|k}.$$

This yields

$$U_j = G_{j|k} - E\Lambda^{j+1} E^{-1} G_{-1|k},$$

where

$$G_{j|k}(\xi_1, \xi_2) = \frac{a_3}{2\pi} \int_{-\pi/a_3}^{\pi/a_3} D(\boldsymbol{\xi})^{-1} e^{i(j-k)a_3\xi_3} d\xi_3.$$

The derivation here assumes $k>0$, i.e., the location of the point force is away from the interface. With a direct calculation, one can verify that the formula is also valid for $k=0$. Finally let

$$A(\xi_1, \xi_2) = E\Lambda E^{-1}.$$

Then the half-space Green's function is now expressed as a Fourier integral

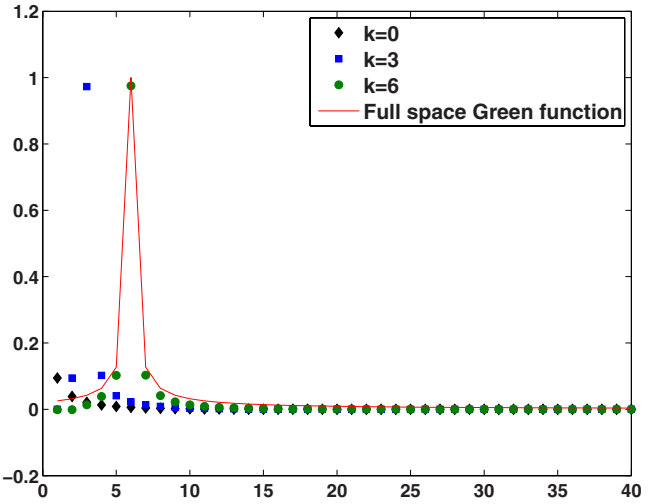

FIG. 4. (Color online) Half-space Green's function. The normal direction is ⟨110⟩. The diagonal (1,1) entries of the Green's functions, centered at $k=0,3$, and 6, are plotted, along with the full-space Green's function for comparison. In these calculations, 128^3 k points are used for the Fourier integral.

$$g^+(ma_1, na_2, la_3|k) = g[ma_1, na_2, (l-k)a_3]$$
$$- \frac{1}{|\mathcal{B}|} \int_{\mathcal{B}} A(\xi_1, \xi_2)^{l+1} D(\boldsymbol{\xi})^{-1} e^{i[ma_1\xi_1 + na_2\xi_2 - (k+1)a_3\xi_3]} d\boldsymbol{\xi},$$
$$= \frac{1}{|\mathcal{B}|} \int_{\mathcal{B}} e^{i[ma_1\xi_1 + na_2\xi_2 + (l-k)a_3\xi_3]}$$
$$\times [I - A(\xi_1, \xi_2)^{l+1} e^{-i(l+1)a_3\xi_3}] D(\boldsymbol{\xi})^{-1} d\boldsymbol{\xi}. \tag{28}$$

In Fig. 4, we plotted the half-space Green's function for a BCC system along the ⟨110⟩ direction. We can observe that as the center moves away from the surface, the half-space Green's function will approach to the full-space Green's function. Therefore, in our variational formulation, these half-space Green's functions are only used when the center is about 10 atomic spacings away from the interface. For points in bulk, the full-space Green's functions are used.

IV. NUMERICAL RESULTS

Both of the following numerical tests are conducted on a BCC iron-α system. For the interatomic potential, we use the embedded atom potential.[27] The lattice parameter is $a_0=2.866$ Å with cut-off distance 8.107 Å, which includes 148 neighbors. Notice that this cut-off distance is larger than that of the electron density, which is 4.095 Å. For the parameter $r_{\min}$ in Eq. (13), we set it to $6a_0$, and for each atom at the boundary, there are about 250 inside atoms within this range. Therefore, the cost of implementing this BC is about the same as the force calculation for each atom for empirical potentials.

A. Single-edge dislocation in iron-α

Our first test is on a single-edge dislocation. We consider a dislocation with Burger's vector $a_0/2\langle 111\rangle$ and slip plane

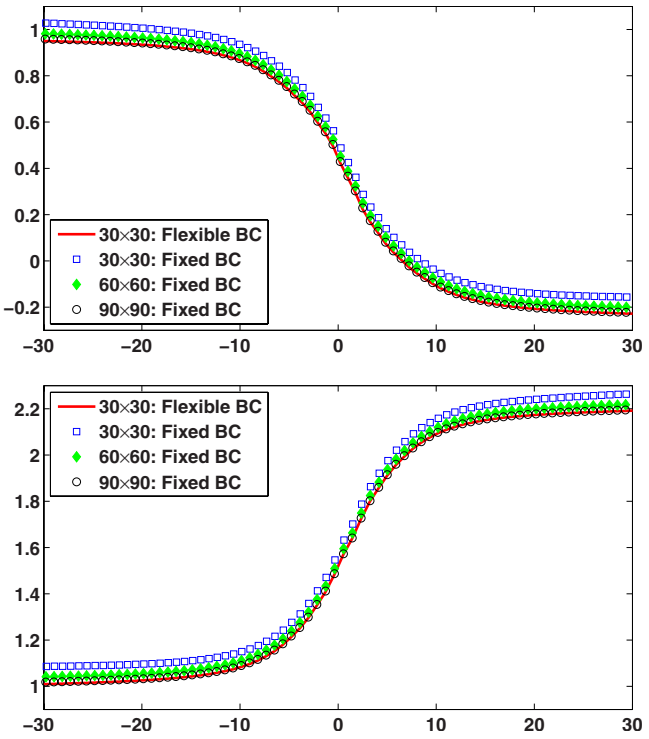

FIG. 5. (Color online) Simulation of a single-edge dislocation. Plotted in the figure is the first component of the displacement just above and below the dislocation line.

{110}. The initial position of the atoms are computed from the analytical solution of the anisotropic elasticity based on the Stroh's formalism.[28] Other studies of such system based on atomistic models can be found, e.g., in Refs. 1, 2, and 29–31. To create the computational domain, we start with a unit cell with six atoms and duplicate the cells in the $\langle 111\rangle$, $\langle 110\rangle$, and $\langle 1\bar{2}1\rangle$ directions. In the third direction, we use 20 cells with periodic boundary conditions applied.

We start with a system with the simulation box of 30×30 cells in the $\langle 111\rangle$ and $\langle 110\rangle$ directions. In the Stroh's formalism, we first choose the line force $f=0$. In this case, our boundary condition produces the same results as the fixed boundary conditions. For a system of this size, this observation agrees with that of many other simulations, e.g., Ref. 2. Next we choose $f=41.42$ GPa Å^2 along the direction of the Burger's vector. In Fig. 5, we show the results from our boundary condition and the fixed boundary condition for different system size. We find that in this case, the results from the fixed boundary condition depend on the system size and they start to converge when the size is increased to about 90×90 and they agree with the results computed from our flexible boundary condition.

In the minimization procedure, we set the following convergence criterion: $\max_i \|\mathbf{f}_i\|_\infty < \mathrm{TOL}$, and $\mathrm{TOL}=10^{-3}\ k_B$ K Å^{-1}. Table I shows the number of iterations and the cpu time for each numerical run.

B. Simulation of an elliptical crack

Next we consider an elliptical crack in the BCC iron-α system. The system studied is a 3D rectangular sample with the three orthogonal axes along the $\langle 110\rangle$, $\langle 1\bar{1}0\rangle$, and $\langle 001\rangle$ directions, respectively. The crack is chosen to lie on the {110} plane and the crack front is parallel to the $\langle 001\rangle$ direction. The initial position of the atoms are computed from the analytical solution of the anisotropic elasticity.[32] In the analytical solution, the length of the crack is chosen to be 10^6 times the atomic spacing, which is one the scale of millimeters. The surface energy, which is needed in the anisotropic solution, is taken as 0.089 eV Å^{-2}.[27]

TABLE I. Number of iterations and the cpu times.

Boundary condition	No. of iterations	cpu time
30×30 fixed BC	81	181 s
60×60 fixed BC	142	1354 s
90×90 fixed BC	222	4680 s
30×30 flexible BC	500	1394

For the analytical solution, one can find a critical value of the stress intensity factor, K_I^*, which predicts the failure criterion for a brittle crack. In the first simulation, we let $K_I=K_I^*$, and the results are displayed in Fig. 6. In this case, the displacement from all the simulations only changes slightly and the crack front stays at the initial position, indicating that the analytical solution of the linear continuum model is a very good approximation. In the simulations with fixed boundary condition, the displacement of the atoms along the crack face does depend on the system size, but the results start to converge as the system size is increased to about 60×60. We then set $K_I=1.2K_I^*$ to create an overloading. In this case, we observe more dependence on the system size for the fixed boundary condition: for simulations with system size 30×30 and 60×60, they do not correctly predict the location of the crack tip. Nevertheless, in both cases, the flexible boundary condition applied to a small system produce results that agree with that from a simulation of a large system.

V. CONCLUSION AND DISCUSSIONS

Based on a consistent harmonic approximation, we have formulated the boundary condition for molecular statics models. With such boundary conditions, we are able to reduce the full model to a problem in a much smaller computational domain. The boundary conditions are expressed as a mapping from the atoms in the computational domain to the outside atoms that are close to the boundary. Comparing to existing methods, the implementation of such boundary condition is very efficient. To compute the boundary condition, lattice Green's functions are used as test functions to guarantee the accuracy. Several implementation issues are discussed. We expect that the boundary condition will be useful for full three-dimensional simulations.

As examples, we conducted numerical tests on systems with dislocations and cracks. In these examples, the predictions from elasticity model are available and they are known to be good approximations for the atomistic model. Therefore, in these cases, the numerical results converge quickly

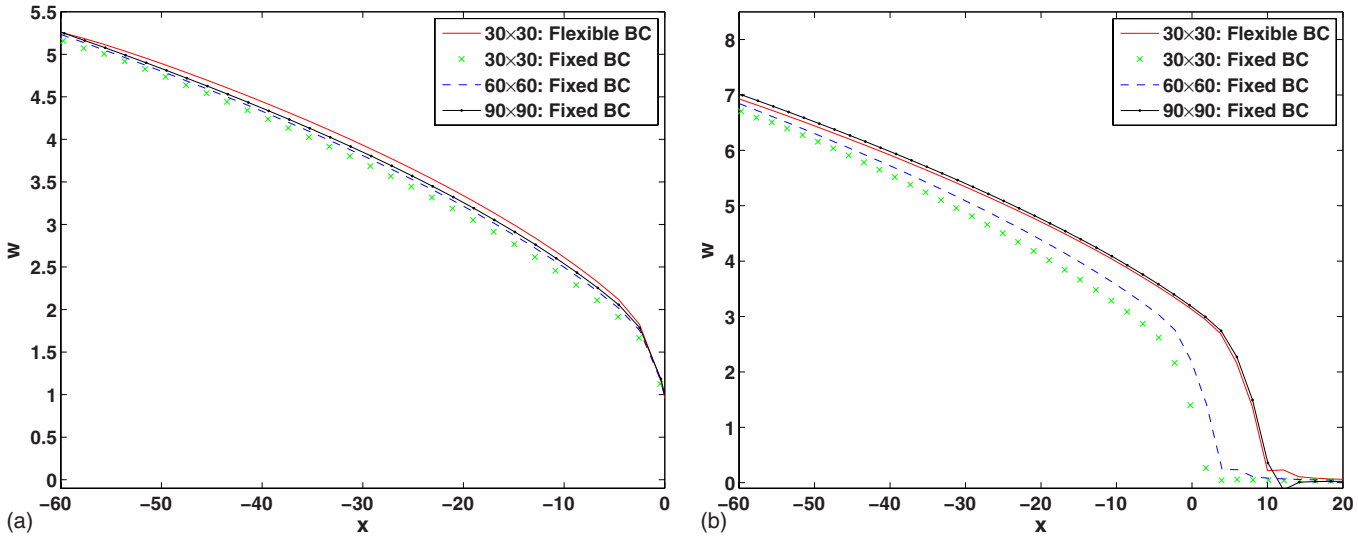

FIG. 6. (Color online) Simulation of an open crack. Plotted in the figure is the third component of displacement along the upper crack face. Left: $K_I=1.0K_I^*$; right: $K_I=1.2K_I^*$.

as the system size increases. As a result, we are able to compare the results computed from the flexible boundary condition to full atomistic results. For problems where the system is away from equilibrium and the continuum solutions are not available, we expect that the role of these boundary conditions will be more critical.

Since the full atomistic model is an optimization problem, the method proposed here can be viewed as a Newton's method, applied for one step. The question of how to make more iterations to improve the accuracy still remains. The more general cases, such as quasistatic loading at the remote boundaries, are difficult to deal with in a single atomistic simulation. They have to be treated either by coupling the atomistic model with a continuum description, or by a coarse-graining method, keeping some selected atoms in the outer region to describe the mechanical deformation. One such example is the quasicontinuum method.[33,34] In the multiscale setting, we expect that the current boundary condition will also play an important role. This will be explored in separate works.

*xli@math.psu.edu

[1] J. E. Sinclair, P. Gehlen, R. G. Hoagland, and J. P. Hirth, J. Appl. Phys. **49**, 3890 (1978).
[2] S. Rao, C. Hernandez, J. P. Simmons, T. A. Parthasarathy, and C. Woodward, Philos. Mag. A **77**, 231 (1998).
[3] J. E. Sinclair, J. Appl. Phys. **42**, 5321 (1971).
[4] D. R. Trinkle, Phys. Rev. B **78**, 014110 (2008).
[5] M. Ghazisaeidi and D. R. Trinkle, Phys. Rev. E **79**, 037701 (2009).
[6] E. Karpov, H. Yu, H. Park, W. K. Liu, Q. J. Wang, and D. Qian, Int. J. Solids Struct. **43**, 6359 (2006).
[7] S. N. Medyanik, E. G. Karpov, and W. K. Liu, J. Comput. Phys. **218**, 836 (2006).
[8] C. Woodward, D. R. Trinkle, L. G. Hector, and D. L. Olmsted, Phys. Rev. Lett. **100**, 045507 (2008).
[9] W. Cai, M. de Koning, V. V. Bulatov, and S. Yip, Phys. Rev. Lett. **85**, 3213 (2000).
[10] W. E and Z. Huang, J. Comput. Phys. **182**, 234 (2002).
[11] W. E and Z. Huang, Phys. Rev. Lett. **87**, 135501 (2001).
[12] E. G. Karpov, G. J. Wagner, and W. K. Liu, Int. J. Numer. Methods Eng. **62**, 1250 (2005).
[13] X. Li, J. Comput. Phys. **227**, 10078 (2008).
[14] X. Li and W. E, Comm. Comp. Phys. **1**, 136 (2006).
[15] A. C. To and S. Li, Phys. Rev. B **72**, 035414 (2005).
[16] B. L. Holian and R. Ravelo, Phys. Rev. B **51**, 11275 (1995).
[17] M. Born and K. Huang, *Dynamical Theory of Crystal Lattices* (Oxford University Press, Oxford, 1998).
[18] N. W. Ashcroft and N. D. Mermin, *Solid State Physics* (Holt, Rinehart and Winston, New York, 1976).
[19] D. Liu and J. Nocedal, Math. Program. Ser. B **45**, 503 (1989).
[20] V. K. Tewary, Adv. Phys. **22**, 757 (1973).
[21] H. J. Monkhorst and J. D. Pack, Phys. Rev. B **13**, 5188 (1976).
[22] R. J. Duffin, Duke Math. J. **20**, 233 (1953).
[23] D. M. Barnett, Phys. Status Solidi **49**, 741 (1972).
[24] E. Pan, ASME J. Appl. Mech. **70**, 101 (2003).
[25] T. C. T. Ting and V.-G. Lee, Mech. Appl. Math. **50**, 407 (1997).
[26] T. Ting, *Anisotropic Elasticity: Theory and Applications* (Oxford, 1997).
[27] V. Shastry and D. Farkas, MRS Symposia Proceedings, Boston, MA, November 27–December 1, 1995 (Oxford University Press, New York, 1996), pp. 75–80.
[28] A. N. Stroh, Philos. Mag. **3**, 625 (1958).
[29] B. L. Adams, J. P. Hirth, P. C. Gehlen, and R. G. Hoagland, J. Phys. F. Met. Phys. **7**, 2021 (1977).
[30] J. Th. M. de Hosson and A. W. Sleeswyk, Solid State Commun. **17**, 245 (1975).
[31] Y. N. Osetsky and D. J. Bacon, Modell. Simul. Mater. Sci. Eng. **11**, 427 (2003).
[32] G. C. Sih and H. Liebowitz, *Fracture, an Advanced Treatise* (Academic, New York, 1968).
[33] E. B. Tadmor, M. Ortiz, and R. Phillips, Philos. Mag. A **73**, 1529 (1996).
[34] J. Knap and M. Ortiz, J. Mech. Phys. Solids **49**, 1899 (2001).